Journal of Alloys and Compounds 585 (2014) 318–324

Contents lists available at ScienceDirect

Journal of Alloys and Compounds

journal homepage: www.elsevier.com/locate/jalcom

Production of Al–Cu–Fe metallic foams without foaming agents or space holders

M.A. Suarez [a], I.A. Figueroa [a,*], G. Gonzalez [a], G.A. Lara-Rodriguez [a], O. Novelo-Peralta [a], I. Alfonso [a], I.J. Calvo [b]

[a] Instituto de Investigaciones en Materiales, Universidad Nacional Autónoma de México (UNAM), Circuito Exterior S/N, Cd. Universitaria, C.P. 04510 México, D.F., Mexico
[b] Facultad de Química, Departamento de Ingenieria Metalúrgica, Universidad Nacional Autónoma de México (UNAM), Circuito Exterior S/N, Cd. Universitaria, C.P. 04510 México, D.F., Mexico

ARTICLE INFO

Article history:
Received 9 May 2013
Received in revised form 30 July 2013
Accepted 2 August 2013
Available online 21 August 2013

Keywords:
Foams
Heat treatments
Macro porosity
Microstructure
Al–Cu–Fe alloy

ABSTRACT

This investigation presents a study on the intrinsic formation of $Al_{68}Cu_{20}Fe_{12}$ alloy foams, i.e. without the need of foaming agents or space holders. This alloy was slowly solidified in the furnace crucible, producing a multiphase microstructure, mainly composed by the λ-$Al_{13}Fe_4$, I-icosahedral, θ-Al_2Cu and ω-Al_7Cu_2Fe phases. Several heat treatments were carried out to a number of as-cast alloy samples in order to produce foams with porosities above 60%. The microstructure, thermal properties, pore morphology and porosity were characterized by means of SEM, DTA, Image analyzer and Archimedes principle, respectively. The highest amount of macro porosity of up to 65% and a density of 1.5 g/cm^3 in the treated sample were found at 900 °C for 360 min. At this temperature, a highly porous structure formed mainly by the λ-$Al_{13}Fe_4$, I-icosahedral and ω-Al_7Cu_2Fe phase was obtained. The proposed mechanism for the intrinsic porosity formation is based on the high amount of liquid phase generated by the melting of the Cu-rich phases and the peritectic reaction. The reaction between the λ-$Al_{13}Fe_4$ and the liquid phases formed the highly dense ω-Al_7Cu_2Fe and I-icosahedral phases. Thus, the space that is left behind caused the highly porous structure in this material.

© 2013 Elsevier B.V. All rights reserved.

1. Introduction

Metal foams are a new type of material that have a wide range of applications due its lightweight, impact energy absorption capacity, air and water permeability, unusual acoustic properties and low thermal conductivity [1]. According to its definition, metallic foams are considered as porous metals with high porosity, ranging from 40 to 98 vol% [2,3]. As a result of the possible combinations of properties that can provide metallic foams, there is a raising need that demands new fabrication methods to control the pore size and distribution. The commonly known manufacturing processes are classified according to the state of matter in which the metal is processed. The most common methods used are bubbling gas through molten metal and addition of foaming agents. The powder metallurgy and infiltration of liquid metal methods are being extensively used for the manufacture of foams with improved properties and practical applications [4,5]. The manufacturing methods of foams formed by no-crystalline (amorphous and quasicrystals) materials are also in development [6].

Quasicrystalline alloys are of interest, since their physical properties differ from those of conventional crystalline solids. These alloys have a combination of physical, thermal and mechanical properties such as low electrical conductivity, low thermal conductivity, good corrosion and oxidation resistance, low friction coefficient, high hardness and brittleness at room temperature [7]. Consequently, these alloys are suitable for several important applications such as hard coatings, thermal barrier coatings, and thermoelectric materials [8,9]. However, the complex multiphase solidification structures of these alloys together with extreme brittleness limit their practical applications.

The icosahedral quasicrystalline phase present in the Al–Cu–Fe alloy is formed by peritectic solidification of high temperature crystalline phases reacting with a liquid phase. This process is necessarily slow, and mostly some crystalline phases are retained out of equilibrium at room temperature together with the quasicrystal [10]. Therefore, an additional heat treatment is necessary to promote the formation of icosahedral quasicrystalline phase [8,11,12]. Due to crystalline and quasicrystalline phases exhibit significant composition and atomic volume differences; the formation of porosity has been reported, but as unwanted effect [13]. Therefore, different ways have been suggested to reduce the porosity to a minimum while pure quasicrystal is obtained. However,

* Corresponding author. Tel.: +52 5556224651; fax: +52 5556161371.
E-mail address: iafiguera@unam.mx (I.A. Figueroa).

0925-8388/$ - see front matter © 2013 Elsevier B.V. All rights reserved.
http://dx.doi.org/10.1016/j.jallcom.2013.08.015

from a different point view, we believe that the use of such "unwanted" effect could be useful for the fabrication of intrinsic (in situ) metallic foams, widening the application field of the quasicrystalline Al–Cu–Fe alloy.

Based on the above, the objective of the present work is to produce Al–Cu–Fe metallic foams with a high percentage of macro porosity. A novel and detailed study on the sequence formation of macro porosity of the Al–Cu–Fe alloys and their quantification is also presented in this work.

2. Experimental procedure

The $Al_{68}Cu_{20}Fe_{12}$ master alloy was prepared with Al, Cu and Fe elements of high purity (>99.95%). The alloy composition is shown in the ternary Al–Cu–Fe phase diagram, Fig. 1 [14]. A total mass of 0.5 kg was melted in an induction furnace under argon (Ar) atmosphere, using an alumina crucible inserted inside of a graphite susceptor. The melted alloy was slowly solidified, at an average cooling rate of 0.05 °C/s, within the furnace, down to room temperature.

The ingot was cut in several rectangular prism shaped samples with dimensions of 1 cm × 1 cm × 0.5 cm (~6 g), for the subsequent heat-treatment. In order to minimize the superficial oxidation, the samples were encapsulated in quartz tubes (internally coated with boron nitride BN, to avoid the Si contamination) and sealed off in Ar. The heat treatments were performed using an electric resistance furnace at 750 °C for 3, 10, 180 and 360 min and at 900 °C for 360 min. After completing the heat treatments, the samples were subsequently air-cooled.

The surface of the samples in the as-cast condition and heat-treated were prepared by conventional metallography techniques. X-ray diffraction (XRD) analysis was carried out in Bruker D8 Advance diffractometer with Cu Kα radiation. Scanning Electron Microscope images were obtained using a FEG Jeol JSM- 7600F microscope operated at 15 kV of accelerating voltage equipped with X-ray energy dispersive analyzer Oxford INCA X-Act. This was done in order to identify the microstructural evolution and to perform punctual microanalysis of areas close-by the pore formations.

To determine the phase transition temperatures of the different phases that constitute the as-cast microstructure, which are related with the formation of the porosity, a Differential Thermal Analysis (DTA) were performed in the temperature range between 400 and 1200 °C with a heating rate of 10 °C/min, by means of a TA instruments SDT Q-600 calorimeter. The characterization of the macro porosity was carried out with a stereographic microscope. The images were analyzed using the image analyzer software "Digital Imaging Solutions Scandium of Olympus", where the shape and area of the pores were determined.

The porosity % was obtained by using the following equation:

$$P = (1 - \rho_e/\rho_t) \times 100 \quad (1)$$

where P is the porosity and ρ_e, ρ_t, are experimental and theoretical densities, respectively. The theoretical density (ρ_t) was calculated, obtaining a value of 4.3 g/cm^3. The experimental density (ρ_e) was obtained by means of the follow Equation (Archimedes principle):

$$\rho_e = (A/A - B)(\rho_0 - \rho_L) + \rho_L \quad (2)$$

where ρ_0 is the water density (0.99823 g/cm^3 at 20 °C), ρ_L is air density (0.0012 g/cm^3), A and B are weight of the sample immerse in air and water, respectively.

3. Results and discussion

3.1. Microstructural characterization of the as-cast alloy

In this section, the analysis of the as-cast sample will be presented and discussed. The study of the as-cast microstructure and thermal properties of the proposed alloy could lead to a plausible explanation of the cause of the in situ pore formation after the heat treatments. The results of the heat-treated samples and pore formation will be addressed in Sections 3.2 and 3.3. Fig. 2 shows the XRD pattern obtained from the as-cast $Al_{68}Cu_{20}Fe_{12}$ alloy. The most intense peaks correspond to the monoclinic λ-$Al_{13}Fe_4$, I-icosahedral, and CsCl type cubic β-AlFe(Cu) and/or τ-AlCu(Fe) phases. Besides these dominant peaks, the peaks related to monoclinic η-AlCu, tetragonal ω-Al_7Cu_2Fe and tetragonal θ-Al_2Cu phases were also detected. Fig. 3 (a and b) shows backscattered electron images of the as-cast Al-Cu–Fe alloy, where a multi-phase microstructure can be observed. In order to identify each phase, a compositional analysis EDS was performed. Table 1 shows the compositions of the different phases in the as-cast microstructure.

It is worth mentioning that the XRD technique is not suitable to distinguish the presence of the stable β phase from the metastable τ phase, since they have similar CsCl type cubic structure and lattice parameters (a = 0.2910 nm). Nevertheless, the phase composition is a better indicator, since the β phase is richer in Fe than τ phase [15,16]. The composition obtained for this phase, $Al_{50.8}Cu_{46.2}Fe_3$, indicates that the Fe content is closer to the composition of the τ phase than the β phase. In addition, the β phase has a high melting temperature (~980 °C), while the τ phase has a low melting temperature (640–700 °C).

Fig. 4 shows the DTA curve of the as-cast alloy during heating from 400 to 1200 °C with a heating rate of 10 °C min^{-1}. The DTA curve showed six endothermic peaks representing the dissolution or melting events of the phases. The first three endothermic peaks registered in the temperature range from 500 to 720 °C corresponded to the melting of the copper-rich phases, as summarized in Table 1.

The first endothermic peak of low intensity (weak) at around 580 °C could be considered as the melting event of the monoclinic η-AlCu phase, (T_f = 560 °C), the second sharp endothermic peak, the most intense, with an onset temperature of 595 °C corresponded to the melting point of the tetragonal θ-Al_2Cu phase (T_f = 591 °C), while the third peak at 720 °C was related to the melting of the metastable τ-AlFe(Cu) phase, whose melting point has been experimentally reported between 643 and 700 °C [15,17]. The last three endothermic peaks of the DTA curve are associated to the melting

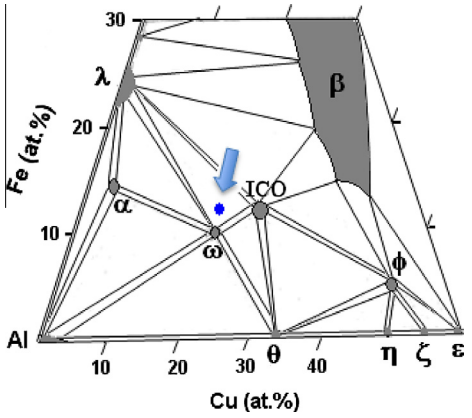

Fig. 1. Portion of the constitutional ternary Al–Cu–Fe diagram at room temperature [14].

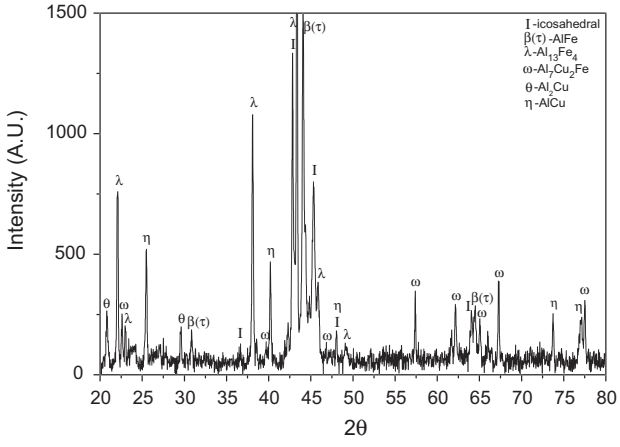

Fig. 2. XRD pattern for the as-cast $Al_{68}Cu_{20}Fe_{12}$ alloy.

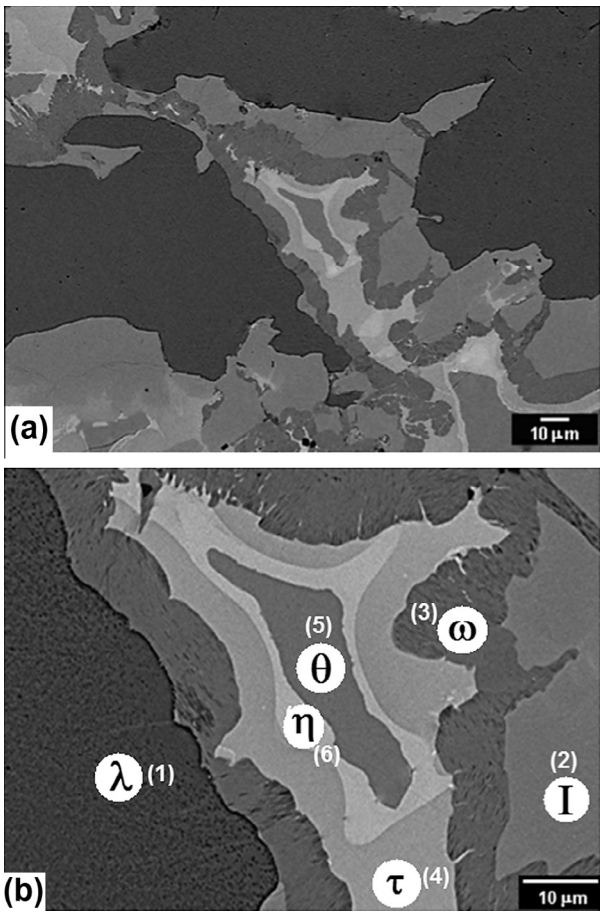

Fig. 3. (a) SEM micrograph of the as-cast alloy and (b) magnification of the central zone.

Table 1
Compositions (EDS), phase related isostructures and melting points for the as-cast alloy.

Point	Composition		Isostructure	Melting points (DTA) (°C)
	at.%	wt.%		
1	$Al_{71.4}$ $Cu_{5.1}$ $Fe_{23.5}$	$Al_{54.1}$ Cu_9 $Fe_{36.9}$	λ-$Al_{13}Fe_4$	1006
2	$Al_{60.1}Cu_{27.9}Fe_{12}$	$Al_{39.8}$ $Cu_{43.7}$ $Fe_{16.5}$	I-Phase	795
3	$Al_{64.9}$ $Cu_{24.9}$ $Fe_{10.2}$	$Al_{44.9}$ $Cu_{40.6}$ $Fe_{14.5}$	ω-Al_7Cu_2Fe	743
4	$Al_{50.8}$ $Cu_{46.2}$ Fe_3	$Al_{30.7}$ $Cu_{65.6}$ $Fe_{3.7}$	τ-AlCu(Fe)	720
5	$Al_{62.4}$ $Cu_{36.9}$ $Fe_{0.7}$	$Al_{41.4}$ $Cu_{57.6}$ Fe_1	θ-Al_2Cu	595
6	$Al_{44.8}$ $Cu_{53.8}$ $Fe_{1.4}$	$Al_{25.8}$ $Cu_{72.8}$ $Fe_{1.4}$	η-AlCu	580

of the rich iron-containing phases. The endothermic peak located at 743 °C corresponded to the melting event of the tetragonal ω-Al_7Cu_2Fe phase (T_f = 740 °C). The penultimate endothermic peak near to 800 °C was related with the melting of the icosahedral phase for this alloy composition. The last endothermic peak at 1006 °C was associated with the melting of the monoclinic λ-$Al_{13}Fe_4$ phase, whose melting point is the highest of all the phases above mentioned. At higher temperatures than 1100 °C, the as-cast alloy was completely melted.

From the SEM-images and DTA (Figs. 3 and 4), it was possible to deduce the solidification sequence of the multiphase microstructure, which is constituted by six phases, in good agreement with the reported in Ref. [18]. The rich iron-containing phases were the first to nucleate and grow, in which the λ-$Al_{13}Fe_4$ dark phase (1) was the first to solidify, followed by the Icosahedral (2) and ω-Al_7Cu_2Fe (3) phases. On the other hand, the phases that contained high copper content such as τ-AlCu(Fe) (4), θ-Al_2Cu (5) and η-AlCu (6) solidified at the end, in the same order.

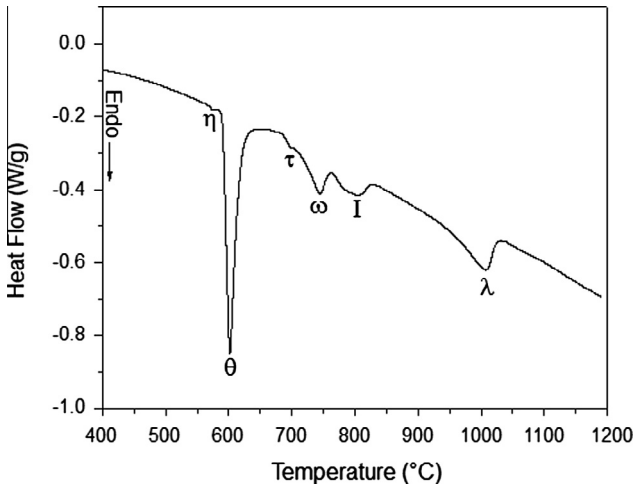

Fig. 4. DTA curve of the as-cast $Al_{68}Cu_{20}Fe_{12}$ alloy showing the melting point of the present phases.

With the SEM-images, the quantification of each phase was carried out using the relative percentage area by means of the image analyzer. The results showed that the λ-$Al_{13}Fe_4$ phase constituted the major part of the microstructure with almost 45%, followed by the icosahedral and θ-Al_2Cu phases with 20 and 15%, respectively. Other phases such as ω-Al_7Cu_2Fe (8%), τ-AlCu(Fe) (7%), and η-AlCu (5%) constituted the balance.

3.2. Microstructural evolution and pore formation at short heat treatments

The composition of the alloy under study is located in the coexistence field of the I-icosahedral, λ-$Al_{13}Fe_4$, ω-Al_7Cu_2Fe and liquid phases, within the isothermal sections at 700 °C and 850 °C, of the ternary Cu–Al–Fe phase diagram [19]. With the heat treatment performed at 750 °C, the transformation kinetics was fast enough that caused a visible formation of liquid phase. Fig. 5a shows the microstructure after 3 min of heat treatment, where the formation of liquid droplets on the surface as well as the beginning of the fusion of a wide zone, next to the liquid droplets, was observed. These first melting events encouraged the initial formation of porosity, which is observed at the bottom of the liquid droplet and the surrounding zone partially melted. According to the EDS microanalysis, the compositions of the liquid drops and the partially molten zone were $Al_{45.8}Cu_{53.2}Fe_1$ and $Al_{63.6}Cu_{35.2}Fe_{1.2}$, which correspond to the composition of the copper-rich η-AlCu and θ-Al_2Cu phases, respectively (Fig. 5b and c). These early melting events are consistent with the results obtained by the DTA curve.

After 10 min of heat treatment at 750 °C, the sample was more homogeneously thermalized, producing a larger amount of liquid phase formed by the gradual melting of copper-rich phases. It is important to mention that no liquid phase was lost from the sample during heat treatment. The presence of the liquid phase in the samples caused two evident effects: (i) phase transformations and (ii) large porosity. The first effect can be observed in Fig. 6a, where the arrows point out the reactions between the liquid and solid phases. The EDS microanalysis performed on the phase transformation events suggested the peritectic reaction between the liquid and the λ-$Al_{13}Fe_4$ phases to form the highly dense ω-Al_7Cu_2Fe phase. Fig. 6b and c shows the peritectic reaction $L + \lambda \rightarrow \omega$ and the microanalysis spectrum of the ω-Al_7Cu_2Fe phase transformation, respectively.

The second effect (large porosity) caused for the formation of the liquid phase can also be observed in Fig. 6a.

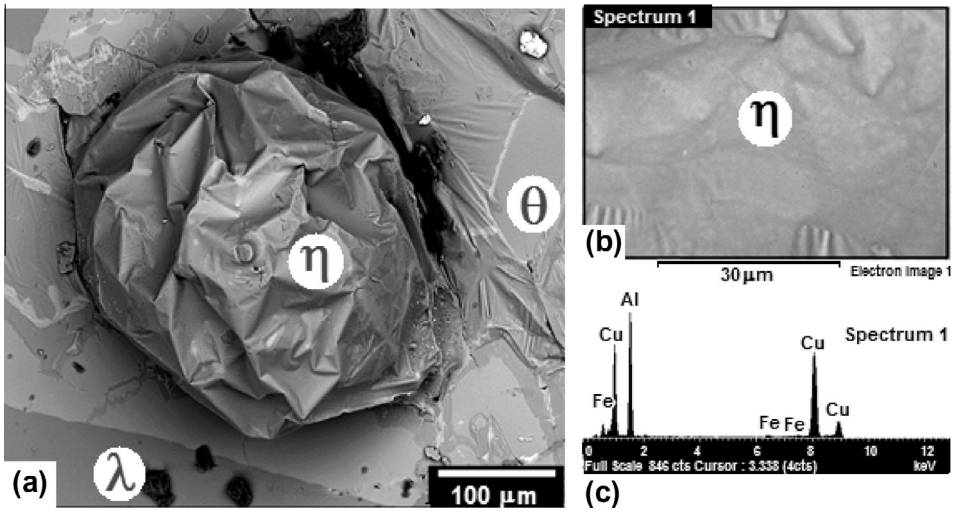

Fig. 5. (a) SEM-micrographs of the alloy after the heat treatment for 3 min; (b), EDS microanalysis on the droplet and (c) EDS spectrum.

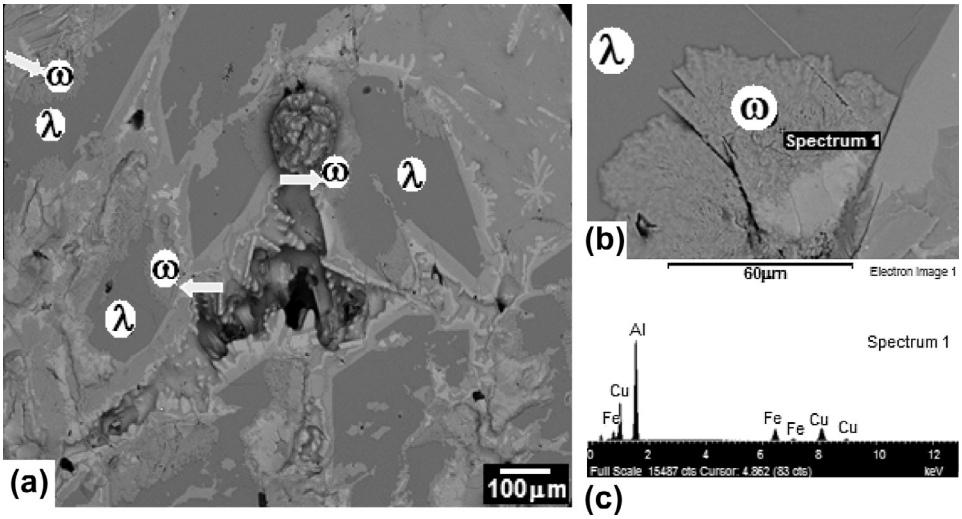

Fig. 6. (a) SEM-micrographs of the alloy after the heat treatment at 750 °C for 10 min; (b) phase transformation (peritectic reaction $L + \lambda \rightarrow \omega$) and (c) EDS microanalysis spectrum.

In a work carried out by Tcherdyntsev et al. [20], the formation of the porosity on a powder consolidated sample of $Al_{65}Cu_{23}Fe_{12}$, after a heat treatment performed at 800 °C was analyzed. They established that the mechanism of porosity formation could be due to the interaction between the solid particles and the liquid phase. In addition, they found that the λ-$Al_{13}Fe_4$ and I-icosahedral phase remained in solid state at 800 °C and the porosity appeared in the Cu-rich region as result of partial melting.

The above-mentioned mechanism could explain the pore formation and phase transformation, with some similitudes of the results presented up to here (Figs. 5a–c and 6a–c). However, heat treatments at longer time and higher temperature could help to provide a deeper insight of the pore formation in this system and this will be presented in Section 3.3.

3.3. Microstructural characterization and large pore formation

From the above, it was noticed the importance of the time and temperature of the heat treatments. It was thought that a possible increment in the percentage of porosity could be achieved by modifying the time and temperature. Note that the temperatures where taken considering the DTA results and the data reported in the literature. The characterization of the samples will firstly be addressed and then, the pore formation will be discussed. Fig. 7 shows the XRD patterns of the alloy after the heat treatments. The diffractogram of the sample (a) treated at 750 °C for 180 min is constituted by the peaks of λ-$Al_{13}Fe_4$, I-icosahedral, ω-Al_7Cu_2Fe and θ-Al_2Cu phases. It was found that sample (b) treated at 750 °C for 360 min was mainly constituted by the I-icosahedral, λ-$Al_{13}Fe_4$, θ-Al_2Cu and ω-Al_7Cu_2Fe phases. While, the diffractogram of the sample (c) treated at 900 °C for 360 min consist of three phases: λ-$Al_{13}Fe_4$, I-icosahedral and ω-Al_7Cu_2Fe. It is worth of mention that the θ-Al_2Cu phase was not detected in the former heat treatment condition. These η-AlCu and τ-AlCu(Fe) phases presented in the as-cast alloy, were not detected after heat treatments.

The SEM images confirmed the above-mentioned XRD results. The microstructure of the sample thermally treated at 750 °C for 180 min showed the presence of I-icosahedral, λ-$Al_{13}Fe_4$, ω-Al_7Cu_2Fe and θ-Al_2Cu phases (Fig. 8a). The formation of the I-icosahedral and the ω-Al_7Cu_2Fe phases was favored with this heat treatment condition, increasing their amount in relation to the as-cast alloy. Moreover, the microstructure of the alloy treated for 360 min consisted of the I-icosahedral and λ-$Al_{13}Fe_4$ phases and by small amount of θ-Al_2Cu and ω-Al_7Cu_2Fe phases (Fig. 8b).

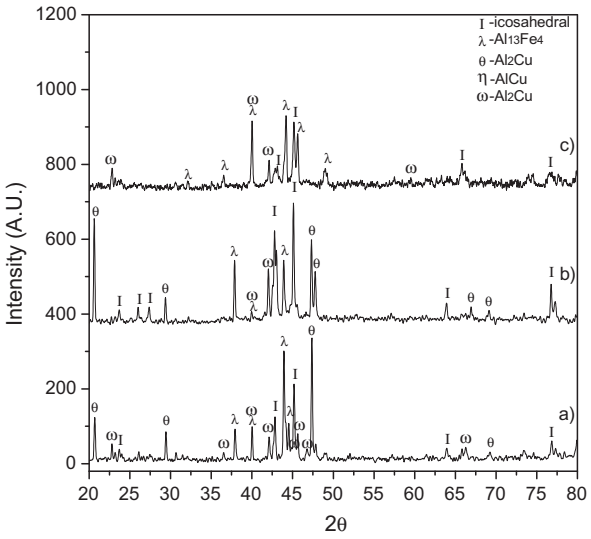

Fig. 7. XRD patterns of the alloy after heat treatments: (a) 750 °C for 180 min, (b) 750 °C for 360 min and (c) 900 °C for 360 min.

The Al–Cu–Fe alloy is frequently thermally treated in the temperature range between 650 and 850 °C to promote the formation of the icosahedral phase [15]. As mentioned above, this composition is located in the coexistence field of the I-icosahedral, λ-Al_{13} Fe_4, ω-Al_7Cu_2Fe and liquid phases, within the isothermal sections at 700 °C and 850 °C, of the ternary Cu–Al–Fe phase diagram [21]. Therefore, as the time of the heat treatments increases, the amount of the I-icosahedral and liquid phases also increases. Besides the predominant aforementioned phases, the θ-Al_2Cu phase was observed in the microstructure. A plausible explanation for this could be attributed to the fact that the cooling air was not fast enough to suppress its formation from the liquid phase. Furthermore, the η- AlCu and τ-AlCu(Fe) phases present in the as-cast alloy were not identified after heat treatments.

When the temperature of heat treatment increased up to 900 °C, the sample was composed by an extremely porous structure formed by the highly dense ω-Al_7Cu_2Fe phase and the I-icosahedral and λ-$Al_{13}Fe_4$ phases, as shown in Fig. 8c. This temperature was chosen based on the DTA curve, as it was noticed that if the temperature of heat treatment increases, for instance at 900 °C, the phases with lower melting temperature than 850 °C, are fully melted. Therefore at 900 °C, the alloy lies between the fully *liquidus* transformation of the I-icosahedral phase and the start of the melting event of the λ-$Al_{13}Fe_4$ phase, i.e. 850 °C and 950 °C, respectively. Kinetically, at higher temperature, the atomic diffusion of the low melting phases is favored; therefore, the heat treatment conducted at 900 °C for 360 min caused a much greater amount of macro porosity and modification of the microstructure. It is thought that the high level of porosity obtained at this temperature

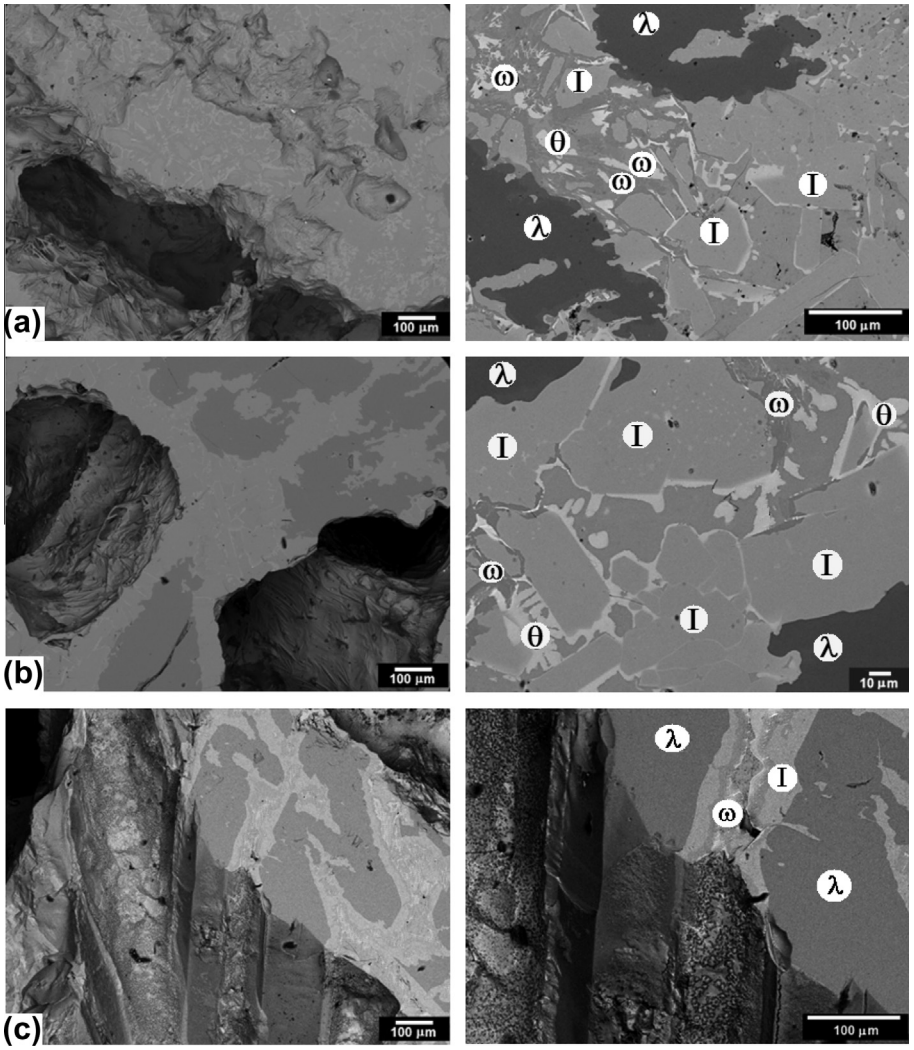

Fig. 8. Macro porosity (left) and microstructure (right) of the alloy treated at: (a) 750 °C for 180 min, (b) 750 °C for 360 min and (c) 900 °C for 360 min.

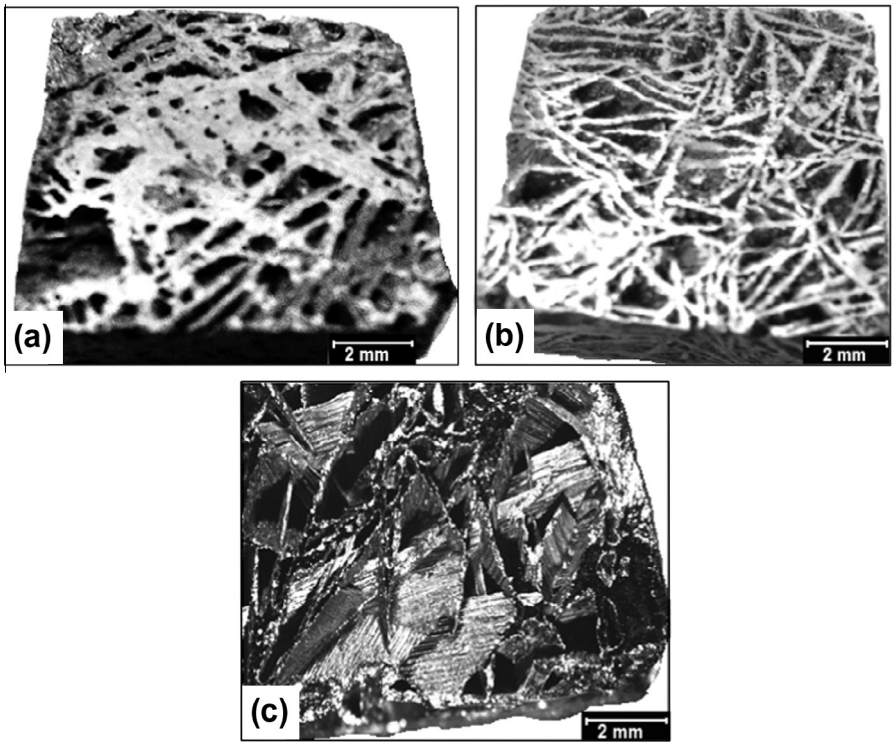

Fig. 9. Resulting $Al_{68}Cu_{20}Fe_{12}$ alloy foams, heat-treated at: (a) T = 750 °C, t = 180 min, (b) T = 750 °C, t = 360 min and (c) T = 900 °C, t = 360 min.

could be attributed to the much higher amount of liquid phase generated by the melting of the ω-Al_7Cu_2Fe, I-icosahedral and Cu-rich phases.

From the same SEM images of Fig. 8a–c, it can be observed that the ingots after heat treatment displayed a microstructure constituted by a large amount of superficial and deep macro pores. Besides the deep macro pores formed from the surface, similar size macro pores were formed throughout the entire ingot, and some of them suggested a degree of interconnection. This was observed by cutting the sample in several slices; although a further analysis is highly necessary to determine, more accurately, the degree of interconnection.

Finally, some techniques used for manufacturing porous materials could produce expansion of the samples as by the powder metallurgy (PM) route [21]. Such expansion has been attributed to the formation of fine Kirkendall porosity (pore size of ~1 μm) [22], which is produced by vacancies generated due to interdiffusion of atoms of pure elements in solid state. In our particular case, the range of porosity is between 0.1 mm and 2 mm; the phase transformations and the presence of high level of porosity did not modify the dimensions of the investigated samples. This suggests that the Kirkendall effect could not be associated to the formation of porosity reported in this work.

3.4. Evaluation of porosity

In order to determine the size and shape of the pores produced after the heat treatments, the aforementioned standard image analysis software was used. Different optical images were taken at low magnification for better assessment of the macro porosity.

Fig. 9a shows the alloy after the heat treatment at 750 °C for 180 min. It can be observed that the samples displayed macro pores with polygonal morphology (if observed in 2D). This morphology could be attributed to resulting network of the λ and icosaedral phases, which were initially formed. Fig. 9b corresponds to the alloy treated at 750 °C for 360 min that also showed the formation of a macro porous morphology, with larger pore size. At this time of heat treatment, the pore area increased 15% when compared with the previous sample (Table 2).

Table 2
Pore average, volumetric porosity and density of the $Al_{68}Cu_{20}Fe_{12}$ foam samples after the heat treatments.

Sample	Pore area (mm^2)			Volumetric porosity (%)	Density (g/cm^3)
	Min	Average	Max		
As-Cast	–	–	–	–	4.3
180 min-750 °C	0.08	0.6	0.85	40	2.57
360 min-750 °C	0.09	0.9	1.15	55	1.93
360 min-900 °C	0.13	1.3	2.39	65	1.5

When increasing the heat-treatment temperature up to 900 °C for 360 min, the macro porosity increased considerably (Fig. 9c). The morphology of the macro pores became much sharper as compared to all previous samples. Table 2 shows the dimensions of the macro porosity obtained in the samples after the heat treatment. It can be observed that when increasing both, time and temperature, the pore area also increased. The sample treated for 360 min at 900 °C reached a pore area $\geqslant$1.3 mm^2. The average size of porosity reported in other works for the Al–Cu–Fe alloys is around 30–300 μm [20,23,24]. The magnitude of porosity generated in this work surpasses all the data reported in the literature for this experimental process and alloy system. The obtained type of the porosity could be considered as intrinsic, since, this porosity was not a result of an external reaction of a foreign substance.

From the density measurements, by means of Eqs. (1) and (2) (Archimedes principle), it was possible to determine the % porosity of the ingots; the results are summarized in Table 2. The calculated and experimentally obtained density of this alloy composition (without porosity) was approximately 4.3 g/cm^3. The macro porosity ratio strongly depended of the as-cast microstructure and the

conditions of heat treatment. The increase of time and temperature of heat treatment caused a decrease of density and an increase in the macro porosity. The density obtained for the sample treated at 900 °C for 360 min was 1.5 g/cm^3, reaching a porosity level $\geqslant$65%.

4. Conclusions

In this work we have reported for the first time the formation of a highly porous structure in the $Al_{68}Cu_{20}Fe_{12}$ alloy without the need of foaming agents or space holders. The highest level of porosity occurred at a heat-treatment temperature of 900 °C for 360 min, with values of macro porosity and density of 65% and 1.5 g/cm^3, respectively. The mechanism of the formation of intrinsic highly porous metallic foam could be attributed to the large shrinkage generated by a peritectic reaction. This reaction formed as structure composed by the highly dense ω-Al_7Cu_2Fe phase and λ-$Al_{13}Fe_4$ and some I-icosahedral phase. This resulted in the formation of macro pores (up to 1.3 mm^2). At present we are exploring several compositions with different Fe and Cu content in order to promote a higher amount of liquid and I-icosahedral phases, with the aim to produce metallic foams with porosities above 65%.

Acknowledgements

The authors would like to acknowledge the financial support from SENER–CONACYT 151496 for funding the project. A. Tejeda-Cruz, J. J. Camacho, J. Morales-Rosales, C. Flores-Morales, M.J. Arellano-Jiménez, C. Delgado, G. Aramburo, D. Cabrero, C. González and E. Sanchéz are also acknowledged for their technical support.

References

[1] M.F. Ashby, A.G. Evans, N.A. Fleck, L.J. Gibson, J.W. Hutchinson, H.N.G. Wadley, Metal Foams: A Design Guide, vol. 1, Butterworth-Heinemann, Boston, 2000.
[2] G.J. Davies, Shu Zhen, Review of metallic foams: their production, properties and applications, J. Mater. Sci. 18 (1983) 1899–1911.
[3] J.A. Gutiérrez-Vázquez, J. Oñoro, Espumas de aluminio Fabricación, propiedades y aplicaciones, Rev. Metal. Madrid 44 (5) (2008) 457–476.
[4] J. Banhart, Manufacture, characterization and application of cellular metals and metal foams, Prog. Mater. Sci. 46 (2001) 559–632.
[5] Muhammad Hussain Ismail, Russell Goodall, Hywel A. Davies, Iain Todd, Formation of microporous NiTi by transient liquid phase sintering of elemental powders, Mater. Sci. Eng. C 32 (2012) 1480–1485.
[6] Jan Schroers, Synthesis method for amorphous metallic foam, J. Appl. Phys. 96 (12) (2004) 7723–7730.
[7] K. Chattopadhyay, K. Biswas, S. Bysakh, G. Phanikumar, Quasicrystalline coatings through laser processing: a study on process optimization and microstructure evolution, Mat. Res. Soc. Symp. Proc. (643) (2001) K15.3.1–K15.3.12.
[8] E. Huttunen-Saarivirta, Microstructure, fabrication and properties of quasicrystalline Al–Cu–Fe alloys: a review, J. Alloys Comp. (363) (2004) 150–174.
[9] J.M. Dubois, S.S. Kang, A. Perrot, Towards applications of quasicrystals, Mater. Sci. Eng. 179A (1994) 122–126.
[10] Pierre Brunet, L.-M. Zhang, Daniel J Sordelet, Matt Besser, Jean-Marie Dubois, Comparative study of microstructural and tribological properties of sintered, bulk icosahedral samples, Mater. Sci. Eng. 294–296 (2000) 74–78.
[11] K.B. Kalmykov, N.L. Zvereva, S.F. Dunaev, N.V. Kazennov, Met. Sci. Heat Treat. 51 (9–10) (2009) 440–443.
[12] K. Biswas, K. Chattopadhyay, Formation of w-Al_7Cu_2Fe phase during laser processing of quasicrystal-forming Al–Cu–Fe alloy, Philos. Mag. Lett. 88 (3) (2008) 219–230.
[13] J.M. Dubois, New prospects from potential applications of quasicrystalline materials, Mater. Sci. Eng. 294–296 (2000) 4–9.
[14] F. Faudot, A. Quivy, Y. Calvayrac, D. Gratias, M. Harmelin, About the AlCuFe icosahedral phase formation, Mater. Sci. Eng. A133 (1991) 383–387.
[15] G.S. Song, M.H. Lee, W.T. Kim, D.H. Kim, Solidification paths for icosahedral quasicrystalline phase in cast $Al_{62}Cu_{25.5}Fe_{12.5}$ and $Al_{55}Cu_{25.5}Fe_{12.5}Be_7$ alloys, J. Non-Cryst. Solids 297 (2002) 254–262.
[16] G.S. Song, E. Fleury, S.M. Lee, W.T. Kim, D.H. Kim, Quasicrystal-forming ability of the icosahedral phase in Al–Cu–Fe–Be alloys, Mater. Sci. Eng. A346 (2003) 42–49.
[17] M. Gogebakan, B. Avar, M. Tarakci, Microstructures and mechanical properties of conventionally solidified $Al_{63}Cu_{25}Fe_{12}$ alloy, J. Alloys Comp. 509S (2011) S316–319.
[18] B. Grushko, R. Wittenberg, D. Holland-Moritz, Solidification of Al–Cu–Fe alloys forming icosahedral phase, J. Mater. Res. 11 (1996) 2177.
[19] V. Raghavan, J. Phase Equilib. Diffus. 26 (1) (2005) 59–64.
[20] V.V. Tcherdyntsev, S.D. Kaloshkin, A.I. Salimon, E.A. Leonova, I.A. Tomilin, J. Eckert, F. Schurack, V.D. Rogozin, S.P. Pisarev, Yu.P. Trykov, Al–Cu–Fe Quasicrystalline Phase Formation by Mechanical Alloying, Mater. Manuf. Process. 17 (6) (2002) 825–841.
[21] H.Y. Gao, Y.H. He, P.Z. Shen, N.P. Xu, J. Zou, Y. Jiang, B.Y. Huang, C.T. Liu, Effect of heating rate on pore structure of porous FeAl material, Powder Metall. 51 (2) (2008) 171–175.
[22] Muhammad Hussain Ismail, Russell Goodall, Hywel A. Davies, Iain Todd, Porous NiTi alloy by metal injection moulding/sintering of elemental powders: Effect of sintering temperature, Mater. Lett. 70 (2012) 142–145.
[23] G.S. Song, S.H. Kim, W.T. Kim, D.H. Kim, Fracture mode for self-fragmentation of carbon contaminated icosahedral Al–Cu–Fe quasicrystalline phase, J. Mater. Sci. Lett. 20 (2001) 1281–1284.
[24] M.A. Suárez, R. Esquivel, J. Alcántara, H. Dorantes, J.F. Chávez, Effect of chemical composition on the microstructure and hardness of Al–Cu–Fe alloy, Mater. Charact. 62 (2011) 917–923.